

Optimize and Reduce: A Top-Down Approach for Image Vectorization

Or Hirschorn*, Amir Jevnisek*, Shai Avidan

School of Electrical Engineering
Tel-Aviv University
Tel-Aviv, Israel

orhirschorn@mail.tau.ac.il, amirjevn@mail.tau.ac.il, avidan@eng.tau.ac.il

Abstract

Vector image representation is a popular choice when editability and flexibility in resolution are desired. However, most images are only available in raster form, making raster-to-vector image conversion (vectorization) an important task. Classical methods for vectorization are either domain-specific or yield an abundance of shapes which limits editability and interpretability. Learning-based methods, that use differentiable rendering, have revolutionized vectorization, at the cost of poor generalization to out-of-training distribution domains, and optimization-based counterparts are either slow (Ma et al. 2022) or produce non-editable and redundant shapes (Li et al. 2020). In this work, we propose Optimize & Reduce (O&R), a top-down approach to vectorization that is both fast and domain-agnostic. O&R aims to attain a *compact* representation of input images by iteratively optimizing Bézier curve parameters and significantly reducing the number of shapes, using a devised importance measure. We contribute a benchmark of five datasets comprising images from a broad spectrum of image complexities - from emojis to natural-like images. Through extensive experiments on hundreds of images, we demonstrate that our method is domain agnostic and outperforms existing works in both reconstruction and perceptual quality for a fixed number of shapes. Moreover, we show that our algorithm is $\times 10$ faster than the state-of-the-art optimization-based method¹.

Introduction

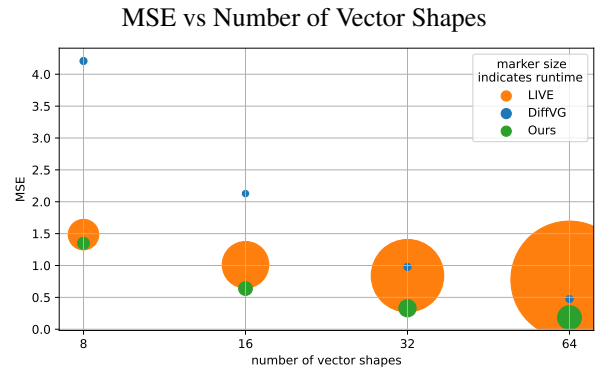
Vectorization refers to the process of transforming a raster image into a vector image. While it is possible to create a vector image with a shape for each pixel, ensuring a perfect reconstruction, this approach lacks compactness and editability. The question arises: can we achieve compact vectorization without compromising quality?

This paper aims to achieve vectorization while minimizing shape count. We show in Figure 1 the tradeoff between shape count and Mean Squared Error (MSE) for our method and two comparative techniques. Our approach demonstrates better performance compared to the state-of-the-art LIVE method (Ma et al. 2022) in both MSE and run-

*These authors contributed equally.

Copyright © 2024, Association for the Advancement of Artificial Intelligence (www.aaai.org). All rights reserved.

¹Code: <https://github.com/ajevnisek/optimize-and-reduce>



- Runtime indicated by marker-size (\downarrow better)

Figure 1: **Optimize & Reduce**: A fast Top-Down approach for raster to vector image conversion, aiming at a low budget of shapes for vectorization. Our method (green circles) achieves lowest MSE error (y -axis) for all shape counts (x -axis) with a low runtime cost (size of circle).

time aspects. Furthermore, our method surpasses DiffVG (Li et al. 2020) in terms of minimizing MSE.

Vector images are an appealing image representation for those seeking infinite resolution and editability. Vector Images are made up of lines and shapes with clear mathematical formulations. A graphical renderer processes the mathematical formulations and renders the image at any specified resolution. This resolution-free property makes them suitable for cases where the image is presented in multiple resolutions, such as commercial logos. A single vector image can be resized to fit the resolution of a business card, a header image in a formal letter, a T-shirt, or a billboard.

The task of vectorization has been studied extensively for many decades (Jimenez and Navalon 1982). We identify two primary drawbacks of classical algorithms for vectorization. First, they are often tailored to a specific domain of images such as fonts (Itoh and Ohno 1993), line drawings (Chiang, Tue, and Leu 1998; Noris et al. 2013), cartoons (Zhang et al. 2009) or cliparts (Favreau, Lafarge, and Bousseau 2017; Dominici et al. 2020). Second, they yield an abundance of shapes making the representation complex. For instance, Potrace (Selinger 2003) generates thousands of

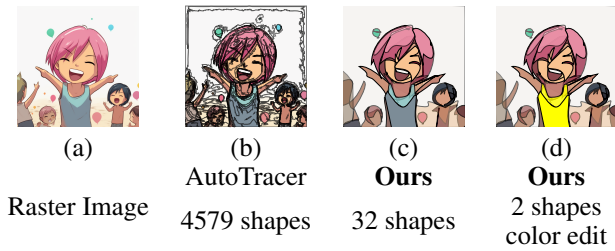


Figure 2: **Low Shapes Budget Vectorization:** Low budget shapes makes editing easier.

shapes for natural-like images.

In contrast, our objective is to achieve a compact vector representation, characterized by a relatively small number of shapes. Intuitively, a low number of shapes enhances the editability of vector images. To demonstrate this we show a comparison between the vectorization of the classical AutoTrace (Weber 2004) and our vectorization approach in Figure 2. Performing a color edit to the shirt is straightforward when the number of shapes is low (32 shapes), whereas, with AutoTrace the task becomes challenging due to the need to augment hundreds of shapes.

Differentiable rasterizers, such as DiffVG (Li et al. 2020), marked a turning point in the field. DiffVG can optimize the vector shape parameters with respect to any raster-based loss function. DiffVG suggested a vanilla vectorization method, directly optimizing the shape parameters. This was extended to two types of vectorization methods: dataset-based and optimization-based approaches. Dataset-based approaches train a neural network to regress the shape parameters and train over some datasets. These methods leverage DiffVG propagation of gradients from the loss function to the shape parameters. Though these methods enjoy a fast inference time, they generalize poorly to out-of-dataset image distribution.

Our focus in this work is to extend Optimization-based methods and provide a method that excels when vectorization runtime and shape compactness are important. While DiffVG (Li et al. 2020) proposes direct optimization for curve parameters, this basic approach is highly sensitive to initialization and tends to generate intricate shapes when optimized using reconstruction or perceptual loss functions. The current State-of-the-art vectorization method in terms of reconstruction error is Layer-wise Image Vectorization (LIVE) (Ma et al. 2022), which employs a bottom-up process to generate a comprehensive set of vectors, achieving layerwise decomposition. However, this advantage comes at the expense of increased runtime, as depicted in Figure 1.

Our approach, Optimize & Reduce (O&R), is a top-down method. Given a raster image, we cluster pixel values to create an initial guess of the shapes. Then, in the *Optimize* step, we use DiffVG to optimize all shapes. We use both reconstruction loss, to match the input raster image, as well as a geometric loss to encourage DiffVG to generate "simple" shapes that do not intersect. In the *Reduce* step, we remove shapes according to an importance measure that we design. The remaining shapes serve as the initial guess for the next

round of optimization. The process is iterated until the target number of shapes is reached. The combination of a smart, clustering-based initialization and our O&R scheme allows DiffVG to optimize for all shapes *at once* leading to excellent results.

Through extensive experimentation, we demonstrate that our approach achieves a runtime speedup of over $\times 10$ compared to LIVE, all while maintaining reconstruction accuracy. Furthermore, we establish that DiffVG produces reconstructions that are inferior to our method, whether initialized randomly (as shown in Figure 1) or with a more informed approach (as illustrated in Figure 17).

We contribute a benchmark of five datasets covering a wide range of image complexities. Three of these datasets consist of images that are typically of interest for vectorization, such as (two versions of) emojis, NFT-apes, and SVG images converted to raster images. The last dataset we propose consists of natural-like images generated by Midjourney. Natural images have also been shown to be of interest for vectorization in previous works (Li et al. 2020; Ma et al. 2022). Thus, our paper’s contribution is threefold: (1) we propose a new vectorization method, (2) through extensive experiments, we demonstrate that our method produces high-quality vector images in terms of reconstruction and perceptual quality, and (3) we provide a benchmark consisting of five diverse image types.

Related Work

Raster To Vector Conversion The conventional image vectorization process typically involves two main steps. Initially, pixels are clustered into regions, either through segmentation or triangulation based on edge detection. Subsequently, these regions are fitted using vector primitives. The optimization in the second step includes both discrete and continuous variables, such as the number and position of primitives. Various exploration mechanisms, like those presented in (Li, Lafarge, and Marlet 2020; Favreau, Lafarge, and Bousseau 2017; Olsen and Gooch 2011) have been proposed for this purpose. Among them, Potrace (Selinger 2003) and Diebel *et al.* (Diebel 2008) utilized an empirical two-stage algorithm to regress segmented components as polygons and bezigons.

In the deep learning era, large, pre-trained models can be employed for pixel clustering, utilizing techniques like semantic segmentation. Moreover, perceptual loss based on deep neural networks can evaluate fitness between image regions and vector primitives. One can categorize vectorization techniques into Dataset-based and Optimization-based.

Some works focus on dataset-level learning, which simplifies the problem to one specific domain of images. Early works used CNNs (Zheng, Jiang, and Huang 2019) or GANs (Balasubramanian, Balasubramanian et al. 2019) to learn a direct conversion between the two representations. Later, Lopes *et al.* (Lopes et al. 2019) and Carlier *et al.* (Carlier et al. 2020) framed the synthesis of vectors as a problem of predicting sequences, whereby the image is represented as a sequence of instructions for drawing, emulating the representation of vector graphics in typical formats.

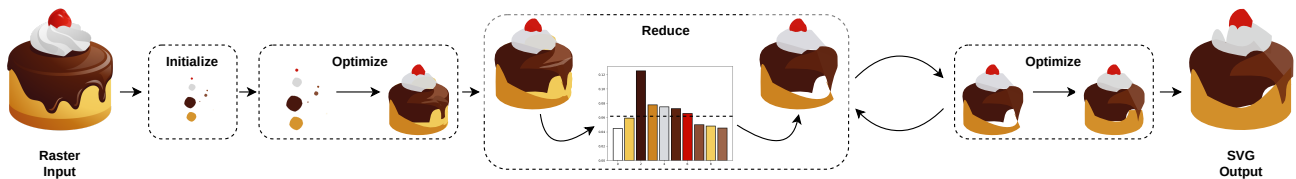


Figure 3: **Optimize & Reduce**: We start with a raster image and use DBSCAN (Ester et al. 1996) and connected components to initialize a large number of Bézier shapes. We **Optimize** the shapes using DiffVG (Li et al. 2020). Then we **Reduce** the number of shapes by ranking them according to \mathcal{L}_{reduce} . That is, the least important k shapes (shapes with scores below the dashed line in the bar graph) are removed. The remaining shapes serve as an initial guess for the next optimization iteration.

Similarly, other works formulate this task as an image-to-image translation using paired data of corresponding images and shape vectors (Yi et al. 2019; Li et al. 2019b,a; Muhammad et al. 2018), which are difficult to acquire. To overcome this supervision problem, there is a popular research trend of integrating differentiable rendering methods (Li et al. 2020; Mihai and Hare 2021) with deep learning models. Reddy *et al.* (Reddy et al. 2021a) suggested a dataset-level method, which utilized differentiable rendering (Li et al. 2020). They used a VAE to encode the input image, and using an RNN network create latent geometric features, which are decoded using a Bézier path decoder and a differentiable rasterizer. However, this method is limited to only a specific domain and performs poorly on complex images. Recently, Jain *et al.* (Jain, Xie, and Abbeel 2022) combined a pre-trained text-to-image diffusion model and a differentiable renderer to create a text-to-vector model. Yet, the topology of the output SVG isn't intuitive, as simple shapes are sometimes represented by multiple overlapping layers.

Meanwhile, optimization-based methods were also suggested, not relying on datasets or lengthy training phases. Vinker *et al.* (Vinker et al. 2022b,a) proposed using semantic Clip objective to optimize Bézier curves for object/scene sketching. Ma *et al.* (Ma et al. 2022) presented a layer-wise image vectorization method, which converts an image to vectors while maintaining its topology, forming shapes that are semantically consistent with the human perspective. They use a differentiable renderer (Li et al. 2020) in a bottom-up approach, optimizing the vector image layer-by-layer. However, this method is extremely slow, as optimizing each layer is compute-intensive. In addition, the output greatly varies according to the initialization method of the shapes, thus becoming a strong prior which fails for complex and texture-rich images. In contrast, our top-down approach is fast, robust to initialization, and can handle both simple and complex images while maintaining editability.

Topology and Editability To ensure easy SVG editing, proper organization, and smooth shapes are crucial. Previous studies have explored image topology for both raster images and vector shapes (Guo et al. 2019; Zhu et al. 2022; Kopf and Lischinski 2011).

Some works study topology, to characterize fonts styles (Wang and Lian 2021; Reddy et al. 2021b; Shimoda et al. 2021), while others use topology as a regularizer for vectorizing sketches (Bessmeltsev and Solomon 2019;

Chan, Durand, and Isola 2022; Mo et al. 2021). For images, early works focused on vectorizing cliparts using various boundary-aware methods (Hoshyari et al. 2018; Dominici et al. 2020; Riso, Sforza, and Pellacini 2022). Later, Favreau *et al.* (Favreau, Lafarge, and Bousseau 2017) and Shen *et al.* (Shen and Chen 2021) decomposed bitmap pictures into gradient-filled vectors, creating visual hierarchy through segmentation and merging. Alternative studies like diffusion curves (Xie et al. 2014; Zhao, Durand, and Zheng 2017; Orzan et al. 2008) and meshes (Sun et al. 2007; Xia, Liao, and Yu 2009; Lai, Hu, and Martin 2009) were explored but fell short for complex scenes.

Reddy *et al.* (Reddy et al. 2021a) proposed simultaneous image vectorization and topology extraction but struggled with shape ordering and domain specificity. Later, Ma *et al.* (Ma et al. 2022) introduced a bottom-up SVG construction with geometric constraints, excelling for basic clipart but struggling with complex images. Our method does not require any pre-segmentation or model training and exhibits a satisfying ability to explore image topologies and create easily editable SVGs, even for complex images.

Image Abstraction The process of abstraction is central to creating a new image. To effectively convey desired details, artists must choose which essential visual characteristics of the subject to depict, and which to exclude (often many). Abstract images maintain semantic essence, exhibiting simplicity with fewer details and textures.

Prior works (Gao et al. 2019; Frans, Soros, and Witkowski 2022; Tian and Ha 2022) used contextual loss for style transfer and vector graphics generation. Li *et al.* (Li et al. 2020) demonstrated the usage of a differentiable renderer with a perceptual loss, to convert images into abstract SVGs. Later, Liu *et al.* (Liu et al. 2021) and Zou *et al.* (Zou et al. 2021) used a differential strokes renderer to produce a series of strokes for a given image, creating abstract paintings of the input image. Vinker *et al.* (Vinker et al. 2022b,a) proposed a semantic CLIP loss for image-to-sketch translation, enhancing semantic fidelity while retaining morphology. ClipVG (Song et al. 2023) used differentiable rendering and CLIP-based optimization to edit images using vector graphics instead of pixels. We follow (Vinker et al. 2022a), demonstrating different levels of abstraction for vectorization tasks, by varying the number of shapes in the output image and by incorporating the suggested CLIP loss as a reconstruction objective.

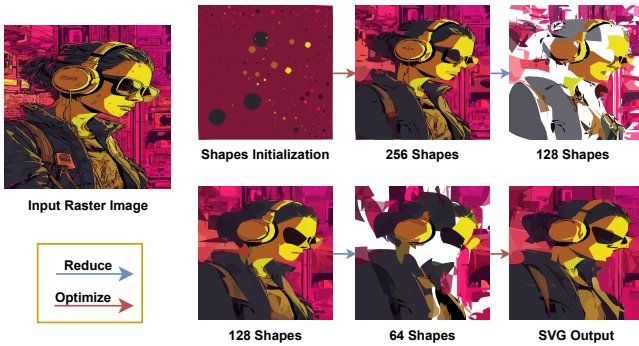


Figure 4: **Algorithm Steps:** We initialize bézier curves sampled uniformly on a circle with a radius inversely proportional to the DBSCAN clusters. We then iterate between optimization and reduction steps for the following schedule: 256 \rightarrow 128 \rightarrow 64. The output SVG reconstructs the raster image with a small number of vector shapes.

Method: Optimize & Reduce

Optimize & Reduce (O&R) is a top-down approach to vectorization that is based on the DiffVG (Li et al. 2020) differentiable renderer. Figures 3 and 4 shows the core steps of our method. We start with a raster image, initialize the shapes and then iterate between Optimize and Reduce. For this scheme to work, we need to define how to initialize the shape parameters, how to determine which shapes to remove, and what loss function to use for DiffVG.

Initialization We found that DiffVG is sensitive to the Bézier curves initialization. Therefore, instead of initializing it with a random set of shape parameters, we use DBSCAN (Ester et al. 1996) to cluster image colors and divide the image into regions that correspond to connected components of each cluster. Then, we sort the connected components according to their pixel area in the source image. The N largest connected components’ center of mass serves as anchors for the differentiable rasterizer. The first optimization step of our method starts with circle-like shapes with a diameter proportional to the connected component area.

Optimize The Optimize step runs DiffVG with the initial guess provided either by the initialization step or the Reduce step (described next). DiffVG takes as input a raster image as well the initial guess of N shapes and optimizes the parameters of all the shapes *at once* to minimize a loss function between the resulting vector image and input raster image.

DiffVG is flexible with the choice of the optimization loss function $\mathcal{L}_{optimize}$, and we evaluate a number of loss functions. These can be any classical reconstruction pixel-wise loss, such as L_1 or L_2 (MSE) loss, as well as a contextualized loss, such as CLIP loss (Vinker et al. 2022b). This loss uses different intermediate layers of CLIP-ViT (Dosovitskiy et al. 2021) where shallow layers preserve the geometry of the image and deeper layers preserve semantics. We also devise a new geometric loss that regularizes the behavior of the Bézier curves, explained later in this paper. Combining

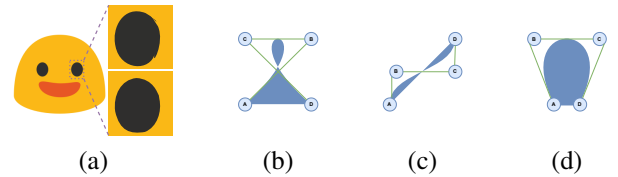


Figure 5: **Geometric Loss:** Our geometric constraint prevents curve intersections, resulting in the smoother topology of shapes. (a) Input image and SVG output without/with (Top/Bottom) geometric regularization. Our geometric loss term has three components, each one aiming to eliminate intersection cases: (b) Self-intersection occurs when AB intersects CD. In addition, Cross-intersections are prone to happen when: (c) $[A, B, C]$ and $[B, C, D]$ have different orientations. (d) $\angle ABC$ or $\angle BCD$ are acute.

all losses results in our general loss term:

$$\mathcal{L}_{optimize} = \mathcal{L}_{reconstruction} + \lambda_{geometric} \mathcal{L}_{geometric} \quad (1)$$

Reduce A shape P is defined via a set of Bézier control points p^k and an RGBA vector c^i . An N -shaped vector image is a set of N shapes: $\{P_i = \{p_i^k, c_i^j\}\}_{i=1}^N$. For each shape P_i , the ranking loss measures the degradation caused by not including that specific shape when the image is rendered. The loss is measured against the original raster image \mathcal{I} . Therefore, the loss for the i -th shape, includes rendering all shapes but the i -th shape:

$$\hat{I} = \text{render}(P \setminus P_i) \quad (2)$$

$$\text{rank-score}[i] = \mathcal{L}_{reduce}(I, \hat{I}) \quad (3)$$

\mathcal{L}_{reduce} can be any classical reconstruction pixel-wise loss, such as L_1 or MSE loss, a contextualized loss, or a non-differentiable loss, such as histogram matching loss. After scoring all shapes, the lower-ranked half of the shapes are removed from the vector representation of the image. The parameters of the remaining shapes serve as the initial guess for the *Optimization* step.

Geometric Loss Term Another contribution of our paper is a geometric loss term that encourages simple shapes through a differentiable penalty for intersections. An example in Figure 5 shows the effectiveness of the proposed geometric loss in mitigating intersection problems. The constraints on the control points prevent the circle shape from intersecting, demonstrating the intuitive and simple, yet highly effective nature of the proposed objective function.

The mathematical formulation is as follows: assume the control points of a cubic Bézier path are (in order): A, B, C, and D. There are two types of intersections: self-intersections, where a single Bézier curve intersects itself, and cross-intersections, where two Bézier curves intersect each other within the same shape. We observed intersections in three scenarios: (a) Self-intersection exists if the lines \vec{AB} and \vec{CD} intersect (Figure 5b). Furthermore, cross-intersections *are prone to happen* when: (b) ABC and



Figure 6: **Dataset Visualization:** We evaluate our algorithm on five datasets: (a) former version of EMOJI (Google 2022) (b) current version of EMOJI (Google 2022) (c) images gathered from free-svg website (d) images from the famous bored apes NFTs (e) images generated using a text-to-image model (Midjourney).

BCD have different orientations (Figure 5c), (c) $\angle ABC$ or $\angle BCD$ are acute (Figure 5d).

To measure self-intersection or orientation change, we compute the orientation (0 is clockwise and 1 is counter-clockwise) of 3 points $[A, B, C]$, where $S(x)$ represents a sigmoid function:

$$O(A, B, C) = S((B_y - A_y) \cdot (C_x - B_x) - (B_x - A_x) \cdot (C_y - B_y)) \quad (4)$$

Using this approximation and simple AND and XOR logic, we can verify the same orientation for $[A, B, C]$ and $[B, C, D]$, or check whether AB intersects CD ($f_{intersect}$ and $f_{orientation}$ defined and detailed in the supplementary). We integrate these functions into our geometric loss:

$$\mathcal{L}_{geom_{ab}} = \lambda_p \cdot (f_{intersect} + f_{orientation}) \quad (5)$$

In addition, The angle loss can be computed using a dot product between the line segments:

$$\mathcal{L}_{geom_c} = ReLU\left(-\frac{AB \cdot BC}{|AB| \cdot |BC|}\right) + ReLU\left(-\frac{BC \cdot CD}{|BC| \cdot |CD|}\right) \quad (6)$$

Our final geometric loss is:

$$\mathcal{L}_{geometric} = \mathcal{L}_{geom_{ab}} + \mathcal{L}_{geom_c} \quad (7)$$

LIVE (Ma et al. 2022) suggests a different geometric loss, that encourages the angle between the first \vec{AB} and the last \vec{CD} control points connections to be greater than 180° . Though this rule encourages shapes to be convex, our loss term also avoids both self-intersection and orientation changes.

Experiments

We introduce five new datasets and compare our method against prior art. O&R is a single-image optimization method, therefore we compare it with single-image methods: DiffVG (Li et al. 2020) and LIVE (Ma et al. 2022). We then demonstrate applications based on our method.

Datasets

For evaluation, we collect five datasets to cover a range of image complexities, including emojis, cliparts, and natural-like images. Figure 6 displays a sample image from each dataset. All datasets will be made publicly available.

EMOJI dataset. We take two snapshots of the NotoEmoji project (Google 2022). The first, taken in 2015, follows LIVE’s EMOJI’s dataset. The second from 2022 introduces color gradients and is available in various resolutions. For evaluation, we resize all of the acquired images to a 240×240 resolution. The supplemental includes a list of all emojis’ names and a showcase of the two datasets.

Free-SVG. A collection of 65 images, including complex clipart images. Compared to the Emoji dataset, this dataset is more complex and difficult for image vectorization.

NFT-Apes. A collection of 100 images from the famous Bored Apes Yacht Club NFT. It features profile pictures of cartoon apes that are generated by an algorithm. It includes images with various backgrounds and complex shapes.

Text-To-Image Generated Images. To stress-test vectorization algorithms we introduce a dataset of images generated by Midjourney, a Text-To-Image public generator. We gather 100 such images alongside their prompts.

Implementation Details

Our code is written in PyTorch (Paszke et al. 2017). Hyperparameters and baseline implementations are described thoroughly in the supplementary.

We use three Reduce steps that follow an exponential decay schedule (i.e., the number of shapes is halved in each iteration). For the qualitative experiments, we use MSE for optimization and L_1 for reduction. All quantitative evaluations use L_1 with our geometric loss for optimization. For reduction, we use L_1 and Clip on Midjourney, and for the other datasets, we use only L_1 . Further details on the runtime analysis are in the supplementary.

Quantitative Evaluation

Figure 1 shows MSE reconstruction error vs the number of vector shapes for the new emoji dataset. Colors in the graph code DiffVG, LIVE, and our method. As can be seen, DiffVG is the fastest but converges to solutions that are not very accurate (especially when the number of shapes is low). LIVE, on the other hand, works well, but takes about 30 minutes² on average to vectorize a 64 shape image. O&R strikes a good balance between the two. It is almost two orders of magnitude faster than LIVE and as accurate. The speedup is a result of our exponential scheduler. For n shapes, LIVE optimizes layer-by-layer which results in $\mathcal{O}(n)$ steps, while we optimize $\mathcal{O}(1)$ steps. For precise runtime figures, please refer to the supplementary materials.

Figure 7 displays the MSE reconstruction error plotted against the number of shapes in the vector representation. Across all datasets, our method consistently outperforms DiffVG with random initialization, when considering the same number of shapes. This observation holds true for the LPIPS score (using VGG (Simonyan and Zisserman 2014)) plotted against the number of shapes, which is presented in the supplemental. It also outperforms DiffVG with our suggested initialization, except for the NFT-Apes dataset, where our DBSCAN initialization introduces a strong in-

²Runtime was measured on an NVIDIA RTX A5000 GPU.

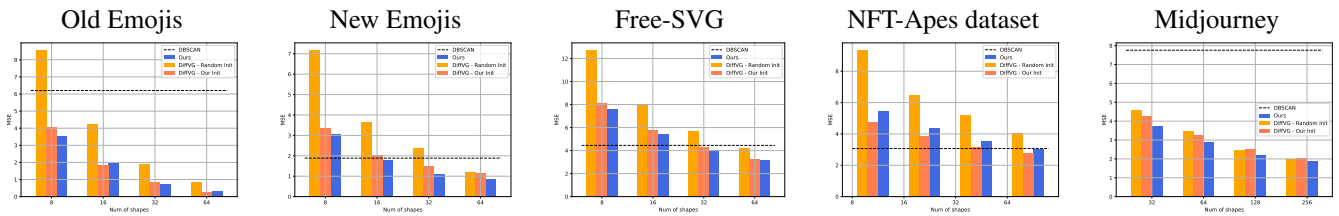


Figure 7: **MSE (\downarrow better) vs Number of shapes:** Our method (blue) outperforms DiffVG with random initialization (orange) for all five datasets. Moreover, using our proposed initialization (peach) improves the performance of DiffVG. Dashed line represents the MSE between DBSCAN-clustering and input image.



Figure 8: **Components Contribution:** Results using 16 shapes. DiffVG is remarkably sensitive to the curve’s initialization, completely missing the party horn.

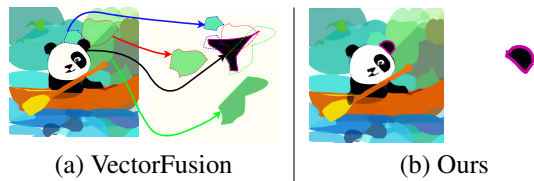


Figure 9: **Convex Shapes: VectorFusion vs Ours :** For VectorFusion, the right ear is composed of not less than four shapes. In our case, the ear is made of one shape. This demonstrates our compact representation and editability.

ductive bias, resulting in improved performance of DiffVG when using our initialization.

Qualitative Evaluation

The Contribution of DBSCAN and O&R Figure 7 shows that DBSCAN initialization reduces DiffVG’s error. However, when a low number of shapes is considered, the introduction of O&R further decreases the error. Figure 17 provides insight into the effectiveness of our components - DBSCAN initialization and O&R optimization scheme. Figures 17(b) and (c) demonstrate DiffVG’s sensitivity to initialization, emphasizing its limitations without effective initialization. Furthermore, the contribution of O&R optimization in mitigating local minima is showcased (Figures 17(c) and (d)). The comparison underscores that DBSCAN initialization alone falls short in yielding semantically satisfactory results for DiffVG. Notably, the primary driver of our algorithm’s success lies in the O&R top-down approach, as demonstrated in Figures 17(d) and (e).

Geometric Loss VectorFusion (Jain, Xie, and Abbeel 2022) is a Text-to-SVG algorithm that given an optimizer

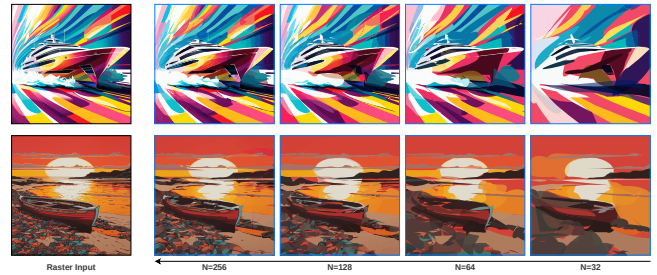


Figure 10: **Results Showcase:** We showcase more results of our method on a collection of images generated using Midjourney. Each image is vectorized using 256, 128, 64, and 32 shapes.

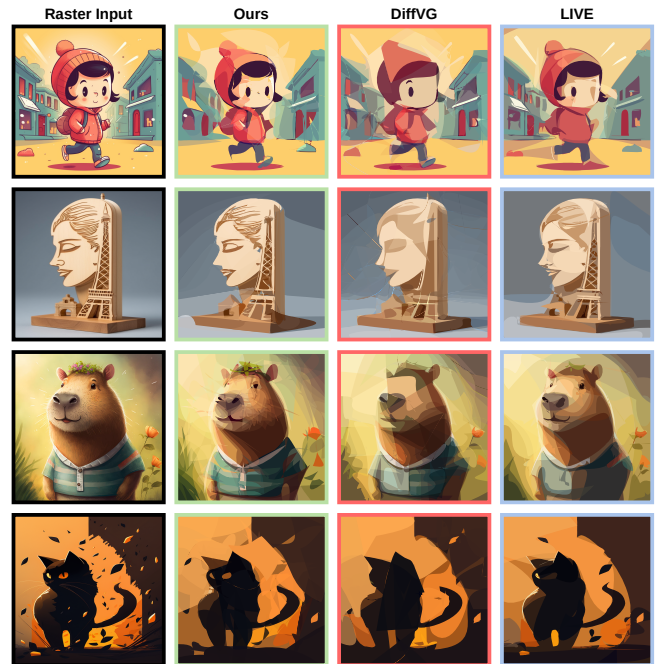


Figure 11: **Qualitative Comparison:** We showcase the results of DiffVG, LIVE, and Our method on a collection of images generated using Midjourney. Each image is compared using the same number of shapes.

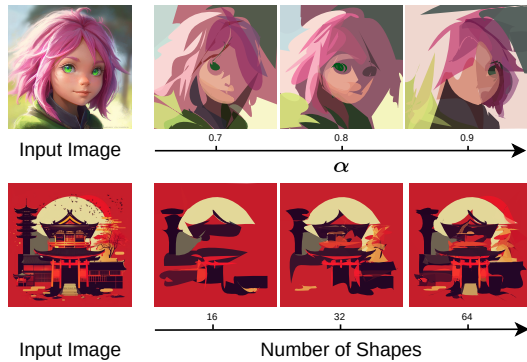


Figure 12: **Abstraction Examples:** Examples of (Top) different levels of abstraction using 16 shapes and various α values and number of shapes. Lower α means more abstraction (Equation 8). (Bottom) various number of shapes.

such as DiffVG (Li et al. 2020) or LIVE (Ma et al. 2022), utilizes a text conditional diffusion model to create an SVG image from a text prompt. Figure 9 shows VectorFusion’s output using LIVE’s framework with its geometric loss and with SDS (Poole et al. 2022) loss, for ”A Panda rowing a boat” prompt. Figure 9a shows LIVE’s decomposition of the shapes composing the panda’s ear. It takes four shapes to capture the ear’s shape. Furthermore, the black shape is non-convex and exhibits a self-intersection. Figure 9b shows the result of taking the image rasterizing it, and vectorizing it with O&R. As highlighted with a pink solid line, we capture the panda’s ear using a single *convex* shape. Additional results and comparisons can be seen in Figures 10 and 11.

Applications

Image Abstraction Inspired by CLIPasso (Vinker et al. 2022b), we demonstrate image abstraction with two degrees of freedom: (1) the number of shapes in the vector image representation, and (2) the extent to which we utilize a CLIP loss for optimization. Accompanied by the Midjourney image prompts, we propose employing CLIP loss, incorporating both its image-to-image components (image embeddings and image attention maps) and text-to-image components.

We define a hyperparameter α in Equation 8, which controls the extent to which a reconstruction loss (L_1 loss) is preferred over a contextualized loss (\mathcal{L}_{CLIP}) when optimizing for shapes parameters. The top row of Figure 12 demonstrates the effect of α on O&R for different values of α . For small values of α the image retains semantic features, whereas for larger values details are neglected, reflecting the effect of L_1 loss.

$$\mathcal{L} = \alpha L_1 + (1 - \alpha) \mathcal{L}_{CLIP} \quad (8)$$

Alternatively, we achieve abstraction with a lower number of shapes as demonstrated in the bottom row of Figure 12. Despite the significant variation in abstraction level, the output SVG remains easily identifiable as depictions of the same input image.

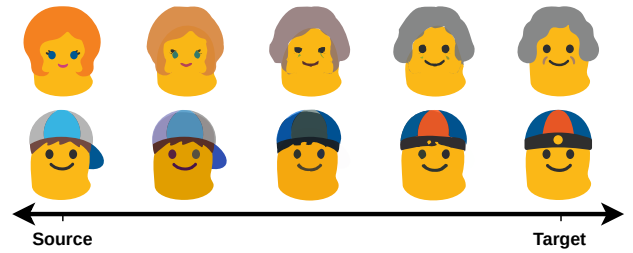


Figure 13: **Interpolation:** We perform an interpolation of emoji images from the rightmost column to the leftmost column. The intermediate images shown in between represent the optimization process’s incremental results.

Interpolation Previous works, such as Im2Vec (Reddy et al. 2021a) and LIVE (Ma et al. 2022), have proposed interpolating emojis and character images in latent space, producing an interpolated latent representation that serves as input to a GAN, which generates a raster image. This raster image is then vectorized to create the vector output. In contrast, our approach does not rely on a GAN to generate interpolated images; instead, it performs interpolation directly in the shapes domain between the source and target images. Our method is preferable as it reflects a realistic scenario where a user wants to interpolate between two emoji images they possess. Our results are achieved without depending on a GAN trained to generate the raster images.

Figure 13 demonstrates an image interpolation application between two emoji images. Interpolating vector images imposes a double correspondence problem: (1) Resolving shape correspondence and (2) Bézier control point correspondence. To overcome this problem, we propose a new mechanism. We start with vectorizing the first image using O&R. Then, we use the vectorized image as the initial approximation for the shape structure and color and optimize the shapes, setting the second image as the target. During optimization, we obtain interpolated states between the two images. We leverage CLIP loss as an optimization objective for O&R to semantically interpolate the two images.

Conclusions

Optimize & Reduce is a top-down approach for vectorization, which excels when the budget of the number of shapes is low. The combination of O&R steps help the algorithm avoid local minima and converge to a solution that minimizes the reconstruction loss. Since O&R is a top-down approach, its’ runtime is much faster than bottom-up approaches. Furthermore, our DBSCAN-based initialization and geometric loss term results in fast and editable results.

As part of our contribution, we suggest a benchmark dataset that facilitates the standardization of vectorization methods. We supplement our demonstrated reconstruction capabilities on this benchmark with applications of image abstraction and emoji interpolation.

Acknowledgments: Parts of this research were supported by ISF grant 1549/19.

References

- Balasubramanian, S.; Balasubramanian, V. N.; et al. 2019. Teaching gans to sketch in vector format. *arXiv preprint arXiv:1904.03620*.
- Bessmeltsev, M.; and Solomon, J. 2019. Vectorization of line drawings via polyvector fields. *ACM Transactions on Graphics (TOG)*, 38(1): 1–12.
- Carlier, A.; Danelljan, M.; Alahi, A.; and Timofte, R. 2020. Deepsvg: A hierarchical generative network for vector graphics animation. *Advances in Neural Information Processing Systems*, 33: 16351–16361.
- Chan, C.; Durand, F.; and Isola, P. 2022. Learning to generate line drawings that convey geometry and semantics. In *Proceedings of the IEEE/CVF Conference on Computer Vision and Pattern Recognition*, 7915–7925.
- Chiang, J. Y.; Tue, S.; and Leu, Y. 1998. A new algorithm for line image vectorization. *Pattern recognition*, 31(10): 1541–1549.
- Diebel, J. 2008. *Bayesian Image Vectorization: The Probabilistic Inversion of Vector Image Rasterization*. Stanford University.
- Dominici, E. A.; Schertler, N.; Griffin, J.; Hoshyari, S.; Sigal, L.; and Sheffer, A. 2020. Polyfit: Perception-aligned vectorization of raster clip-art via intermediate polygonal fitting. *ACM Transactions on Graphics (TOG)*, 39(4): 77–1.
- Dosovitskiy, A.; Beyer, L.; Kolesnikov, A.; Weissenborn, D.; Zhai, X.; Unterthiner, T.; Dehghani, M.; Minderer, M.; Heigold, G.; Gelly, S.; Uszkoreit, J.; and Houlsby, N. 2021. An Image is Worth 16x16 Words: Transformers for Image Recognition at Scale. *arXiv:2010.11929*.
- Ester, M.; Kriegel, H.-P.; Sander, J.; Xu, X.; et al. 1996. A density-based algorithm for discovering clusters in large spatial databases with noise. In *kdd*, volume 96, 226–231.
- Favreau, J.-D.; Lafarge, F.; and Bousseau, A. 2017. Photo2clipart: Image abstraction and vectorization using layered linear gradients. *ACM Transactions on Graphics (TOG)*, 36(6): 1–11.
- Frans, K.; Soros, L.; and Witkowski, O. 2022. Clipdraw: Exploring text-to-drawing synthesis through language-image encoders. *Advances in Neural Information Processing Systems*, 35: 5207–5218.
- Gao, Y.; Guo, Y.; Lian, Z.; Tang, Y.; and Xiao, J. 2019. Artistic glyph image synthesis via one-stage few-shot learning. *ACM Transactions on Graphics (TOG)*, 38(6): 1–12.
- Google. 2022. Noto Emoji.
- Guo, Y.; Zhang, Z.; Han, C.; Hu, W.; Li, C.; and Wong, T.-T. 2019. Deep line drawing vectorization via line subdivision and topology reconstruction. In *Computer Graphics Forum*, volume 38, 81–90. Wiley Online Library.
- Hoshyari, S.; Alberto Dominici, E.; Sheffer, A.; Carr, N.; Ceylan, D.; Wang, Z.; and Shen, I.-C. 2018. Perception-Driven Semi-Structured Boundary Vectorization. *ACM Transaction on Graphics*, 37(4).
- Itoh, K.; and Ohno, Y. 1993. A curve fitting algorithm for character fonts. *Electronic publishing*, 6(3): 195–205.
- Jain, A.; Xie, A.; and Abbeel, P. 2022. VectorFusion: Text-to-SVG by Abstracting Pixel-Based Diffusion Models. *arXiv:2211.11319*.
- Jimenez, J.; and Navalon, J. L. 1982. Some experiments in image vectorization. *IBM Journal of research and Development*, 26(6): 724–734.
- Kingma, D. P.; and Ba, J. 2014. Adam: A method for stochastic optimization. *arXiv preprint arXiv:1412.6980*.
- Kopf, J.; and Lischinski, D. 2011. Depixelizing pixel art. In *ACM SIGGRAPH 2011 papers*, 1–8.
- Lai, Y.-K.; Hu, S.-M.; and Martin, R. R. 2009. Automatic and topology-preserving gradient mesh generation for image vectorization. *ACM Transactions on Graphics (TOG)*, 28(3): 1–8.
- Li, M.; Lafarge, F.; and Marlet, R. 2020. Approximating shapes in images with low-complexity polygons. In *Proceedings of the IEEE/CVF Conference on Computer Vision and Pattern Recognition*, 8633–8641.
- Li, M.; Lin, Z.; Mech, R.; Yumer, E.; and Ramanan, D. 2019a. Photo-sketching: Inferring contour drawings from images. In *2019 IEEE Winter Conference on Applications of Computer Vision (WACV)*, 1403–1412. IEEE.
- Li, T.-M.; Lukáč, M.; Gharbi, M.; and Ragan-Kelley, J. 2020. Differentiable vector graphics rasterization for editing and learning. *ACM Transactions on Graphics (TOG)*, 39(6): 1–15.
- Li, Y.; Fang, C.; Hertzmann, A.; Shechtman, E.; and Yang, M.-H. 2019b. Im2pencil: Controllable pencil illustration from photographs. In *Proceedings of the IEEE/CVF Conference on Computer Vision and Pattern Recognition*, 1525–1534.
- Liu, S.; Lin, T.; He, D.; Li, F.; Deng, R.; Li, X.; Ding, E.; and Wang, H. 2021. Paint transformer: Feed forward neural painting with stroke prediction. In *Proceedings of the IEEE/CVF international conference on computer vision*, 6598–6607.
- Lopes, R. G.; Ha, D.; Eck, D.; and Shlens, J. 2019. A learned representation for scalable vector graphics. In *Proceedings of the IEEE/CVF International Conference on Computer Vision*, 7930–7939.
- Ma, X.; Zhou, Y.; Xu, X.; Sun, B.; Filev, V.; Orlov, N.; Fu, Y.; and Shi, H. 2022. Towards layer-wise image vectorization. In *Proceedings of the IEEE/CVF Conference on Computer Vision and Pattern Recognition*, 16314–16323.
- Mihai, D.; and Hare, J. 2021. Differentiable drawing and sketching. *arXiv preprint arXiv:2103.16194*.
- Mo, H.; Simo-Serra, E.; Gao, C.; Zou, C.; and Wang, R. 2021. General virtual sketching framework for vector line art. *ACM Transactions on Graphics (TOG)*, 40(4): 1–14.
- Muhammad, U. R.; Yang, Y.; Song, Y.-Z.; Xiang, T.; and Hospedales, T. M. 2018. Learning deep sketch abstraction. In *Proceedings of the IEEE Conference on Computer Vision and Pattern Recognition*, 8014–8023.
- Noris, G.; Hornung, A.; Sumner, R. W.; Simmons, M.; and Gross, M. 2013. Topology-driven vectorization of clean line

- drawings. *ACM Transactions on Graphics (TOG)*, 32(1): 1–11.
- Olsen, S.; and Gooch, B. 2011. Image simplification and vectorization. In *Proceedings of the ACM SIGGRAPH/Eurographics Symposium on Non-Photorealistic Animation and Rendering*, 65–74.
- Orzan, A.; Bousseau, A.; Winnemöller, H.; Barla, P.; Thollot, J.; and Salesin, D. 2008. Diffusion curves: a vector representation for smooth-shaded images. *ACM Transactions on Graphics (TOG)*, 27(3): 1–8.
- Paszke, A.; Gross, S.; Chintala, S.; Chanan, G.; Yang, E.; DeVito, Z.; Lin, Z.; Desmaison, A.; Antiga, L.; and Lerer, A. 2017. Automatic differentiation in PyTorch. In *NIPS-W*.
- Poole, B.; Jain, A.; Barron, J. T.; and Mildenhall, B. 2022. Dreamfusion: Text-to-3d using 2d diffusion. *arXiv preprint arXiv:2209.14988*.
- Reddy, P.; Gharbi, M.; Lukac, M.; and Mitra, N. J. 2021a. Im2vec: Synthesizing vector graphics without vector supervision. In *Proceedings of the IEEE/CVF Conference on Computer Vision and Pattern Recognition*, 7342–7351.
- Reddy, P.; Zhang, Z.; Wang, Z.; Fisher, M.; Jin, H.; and Mitra, N. 2021b. A multi-implicit neural representation for fonts. *Advances in Neural Information Processing Systems*, 34: 12637–12647.
- Riso, M.; Sforza, D.; and Pellacini, F. 2022. pOp: Parameter Optimization of Differentiable Vector Patterns. In *Computer Graphics Forum*, volume 41, 161–168. Wiley Online Library.
- Selinger, P. 2003. Potrace: a polygon-based tracing algorithm.
- Shen, I.-C.; and Chen, B.-Y. 2021. Clipgen: A deep generative model for clipart vectorization and synthesis. *IEEE Transactions on Visualization and Computer Graphics*, 28(12): 4211–4224.
- Shimoda, W.; Haraguchi, D.; Uchida, S.; and Yamaguchi, K. 2021. De-rendering stylized texts. In *Proceedings of the IEEE/CVF International Conference on Computer Vision*, 1076–1085.
- Simonyan, K.; and Zisserman, A. 2014. Very deep convolutional networks for large-scale image recognition. *arXiv preprint arXiv:1409.1556*.
- Song, Y.; Shao, X.; Chen, K.; Zhang, W.; Jing, Z.; and Li, M. 2023. CLIPVG: Text-Guided Image Manipulation Using Differentiable Vector Graphics. In *Proceedings of the AAAI Conference on Artificial Intelligence*, volume 37, 2312–2320.
- Sun, J.; Liang, L.; Wen, F.; and Shum, H.-Y. 2007. Image vectorization using optimized gradient meshes. *ACM Transactions on Graphics (TOG)*, 26(3): 11–es.
- Tian, Y.; and Ha, D. 2022. Modern evolution strategies for creativity: Fitting concrete images and abstract concepts. In *Artificial Intelligence in Music, Sound, Art and Design: 11th International Conference, EvoMUSART 2022, Held as Part of EvoStar 2022, Madrid, Spain, April 20–22, 2022, Proceedings*, 275–291. Springer.
- Vinker, Y.; Alaluf, Y.; Cohen-Or, D.; and Shamir, A. 2022a. CLIPascene: Scene Sketching with Different Types and Levels of Abstraction. *arXiv preprint arXiv:2211.17256*.
- Vinker, Y.; Pajouheshgar, E.; Bo, J. Y.; Bachmann, R. C.; Bermanno, A. H.; Cohen-Or, D.; Zamir, A.; and Shamir, A. 2022b. Clipasso: Semantically-aware object sketching. *ACM Transactions on Graphics (TOG)*, 41(4): 1–11.
- Wang, Y.; and Lian, Z. 2021. DeepVecFont: Synthesizing high-quality vector fonts via dual-modality learning. *ACM Transactions on Graphics (TOG)*, 40(6): 1–15.
- Weber, M. 2004. Autotrace-converts bitmap to vector graphics.
- Xia, T.; Liao, B.; and Yu, Y. 2009. Patch-based image vectorization with automatic curvilinear feature alignment. *ACM Transactions on Graphics (TOG)*, 28(5): 1–10.
- Xie, G.; Sun, X.; Tong, X.; and Nowrouzezahrai, D. 2014. Hierarchical diffusion curves for accurate automatic image vectorization. *ACM Transactions on Graphics (TOG)*, 33(6): 1–11.
- Yi, R.; Liu, Y.-J.; Lai, Y.-K.; and Rosin, P. L. 2019. Apdrawngan: Generating artistic portrait drawings from face photos with hierarchical gans. In *Proceedings of the IEEE/CVF conference on computer vision and pattern recognition*, 10743–10752.
- Zhang, R.; Isola, P.; Efros, A. A.; Shechtman, E.; and Wang, O. 2018. The unreasonable effectiveness of deep features as a perceptual metric. In *Proceedings of the IEEE conference on computer vision and pattern recognition*, 586–595.
- Zhang, S.-H.; Chen, T.; Zhang, Y.-F.; Hu, S.-M.; and Martin, R. R. 2009. Vectorizing cartoon animations. *IEEE Transactions on Visualization and Computer Graphics*, 15(4): 618–629.
- Zhao, S.; Durand, F.; and Zheng, C. 2017. Inverse diffusion curves using shape optimization. *IEEE transactions on visualization and computer graphics*, 24(7): 2153–2166.
- Zheng, N.; Jiang, Y.; and Huang, D. 2019. Strokenet: A neural painting environment. In *International Conference on Learning Representations*.
- Zhu, H.; Cao, J.; Xiao, Y.; Chen, Z.; Zhong, Z.; and Zhang, Y. J. 2022. TCB-spline-based Image Vectorization. *ACM Transactions on Graphics (TOG)*, 41(3): 1–17.
- Zou, Z.; Shi, T.; Qiu, S.; Yuan, Y.; and Shi, Z. 2021. Stylized neural painting. In *Proceedings of the IEEE/CVF Conference on Computer Vision and Pattern Recognition*, 15689–15698.

Supplementary

Optimize & Reduce

Optimize & Reduce stated formally: Algorithm 1 provides a comprehensive outline of the Optimize & Reduce (O&R) algorithm. We define explicit functions for the two steps of our method and describe how they are orchestrated to achieve our goal. The algorithm begins with a raster image and utilizes DBSCAN for initialization. We then iteratively perform the Optimize and Reduce steps.

Algorithm 1: Algorithm of Optimize & Reduce

Input: I , shapes, iters
Output: SVG
Function Optimize (I, P):

```

for  $j = 1$  to  $t$  do
     $\hat{I} = \text{render}(P)$ ;
     $\mathcal{L} = \mathcal{L}_{\text{optimize}}(I, \hat{I}, P)$ ;
     $P = P - \alpha \frac{d\mathcal{L}(P)}{dP}$ ; // update shapes
end
return  $P$ ;
Function Reduce ( $I, P, n$ ):
     $L = []$ ;
    for  $j = 1$  to  $\text{len}(P)$  do
         $\hat{I} = \text{render}(P \setminus P[j])$ ;
         $\text{loss} = \mathcal{L}_{\text{reduce}}(I, \hat{I}, P)$ ;
         $L = \text{concat}([L; \text{loss}])$ ;
    end
     $\text{prob} = \text{SoftMax}(L)$ ;
     $P = \text{Sample}(P, \text{prob}, n)$ ; // sample n
    shapes
return  $P$ ;
 $P = \text{init}(I, 2^{\text{iters}} \cdot \text{shapes})$ ;
 $P = \text{Optimize}(I, P)$ ;
for  $n$  in  $[2^{\text{iters}-1} \cdot \text{shapes}, \dots, 2 \cdot \text{shapes}, \text{shapes}]$  do
     $P = \text{Reduce}(I, P, n)$ ;
     $P = \text{Optimize}(I, P)$ ;
end

```

Stochastic Reduce Instead of deterministically removing the bottom half of shapes, we can use sampling to introduce variability. We convert the rank scores to a probability distribution with SoftMax:

$$\text{SoftMax}(z)_i = \frac{e^{z_i/T}}{\sum_{j=1}^N e^{z_j/T}} \text{ for } i = 1, 2, \dots, N \quad (9)$$

We control the extent of variability through the hyperparameter T . Smaller values of T bias the SoftMax operation towards deterministic sampling, where the top-k most important shapes are selected. Conversely, larger values of T lead to sampling under a uniform distribution regime. Figure 14 shows examples of different results created using the same stochastic reduce.

Adding Shapes O&R leverages DiffVG to optimize shape parameters and incorporates a Reduce step to avoid local

Algorithm 2: Probabilistic Reduce

Function Probabilistic-Reduce (I, P, n):

```

shape-score = [];
for  $j = 1$  to  $\text{len}(P)$  do
     $\hat{I} = \text{render}(P \setminus P[j])$ ;
    shape-score[ $j$ ]  $\leftarrow \mathcal{L}_{\text{reduce}}(I, \hat{I})$ ;
end
 $\text{prob} = \text{SoftMax}(L)$ ;
 $P = \text{Sample}(P, \text{prob}, n)$ ; // sample n
shapes
return  $P$ ;

```

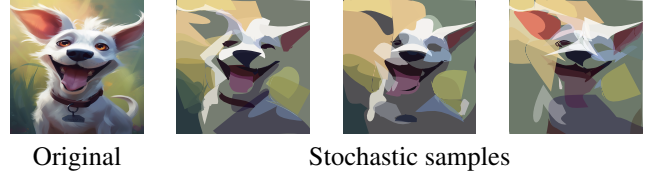


Figure 14: **Reduction Sampling:** Results of different runs for the same input configuration, due to the stochastic nature of our reduce step. We reduce the number of shapes drastically to emphasize the effect of the sampling.

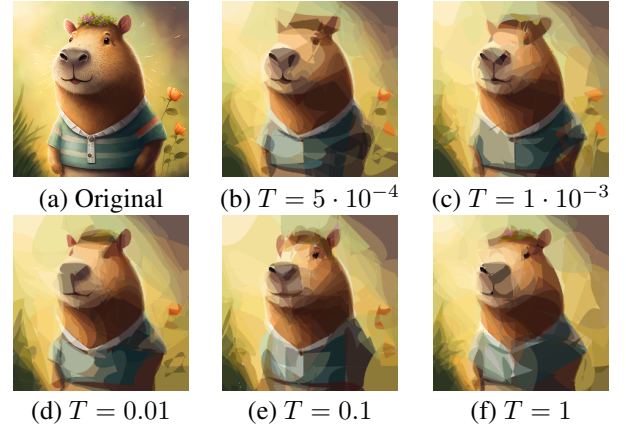


Figure 15: **Sampling Temperature:** Results using different SoftMax temperatures. Lower temperature means more deterministic sampling

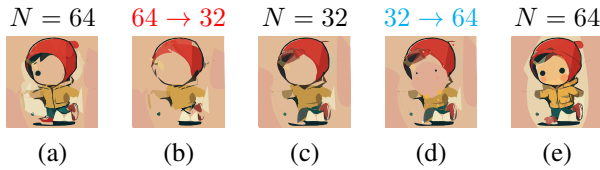


Figure 16: **Add Operation:** We run O&R with a schedule of: $256 \rightarrow 128 \rightarrow 64 \rightarrow 32 \rightarrow 64$ shapes. (a) illustrates the Optimization process to 64 shapes, (b) demonstrates the Reduce step to 32 shapes, (c) displays the optimization of 32 shapes, (d) shows the initialization of 32 additional Bézier shapes, and (e) exhibits the result of the Add operation, bringing the shape count back to 64. Once the foundation of 32 shapes is established, adding 32 shapes captures previously missing details like the subject’s eyes and cheek blush.

minima. We employ an exponential Reduce scheduler that halves the number of Bézier shapes in each iteration. However, for images with intricate details or prominent textures, a low number of shapes leads to coarse segmentation. To enhance the representation of textures and preserve fine details, we introduce an *Add* operation. Inspired by LIVE (Ma et al. 2022), we selectively add shapes to regions with high reconstruction error and optimize these newly added shapes, all at once, using DiffVG. Figure 16 illustrates how the add operation boosts performance. Adding 32 shapes back after O&R to 32 shapes adds back the subjects’ eyes and cheek blush.

Initialization: We emphasize the importance of a robust initialization method for initializing Bézier shapes, as it plays a vital role in the differentiable rendering-based image vectorization process. Our initialization technique is based on DBSCAN, a clustering algorithm that does not require a prior assumption on the number of clusters. In the main paper, we compare the Mean Squared Error (MSE) with the number of shapes for DiffVG using random initialization, DiffVG using our initialization, and Our method. Through this graph, we quantitatively demonstrate our dual contribution, showcasing consistent improvement from DiffVG with random initialization to DiffVG with our initialization. Additionally, for all datasets except NFT-Apes, transitioning from DiffVG to O&R as the optimization method, leads to further enhancements in reconstruction results. For a qualitative assessment, we direct the reader to Figure 17, which illustrates the impact of our initialization. Without our initialization, DiffVG with random initialization fails to capture important shapes in the image such as the mouth and eyes. Our initialization aids in recovering the mouth region, while with O&R, with the same final shape budget, we successfully reconstruct all facial attributes of the emoji.

Image Editing Figure 18 illustrates color editing for two example images. The left triplet displays (a) the original raster image, (b) the application of O&R, and (c) a color edit in which the flame color has been changed. This color edit involved modifying a *single shape* parameter. The right triplet demonstrates a color edit performed on the object’s

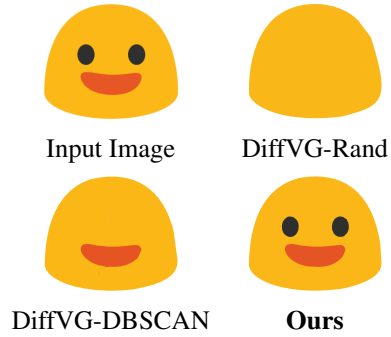


Figure 17: **DBSCAN Initialization Contribution:** Results using 4 shapes. DiffVG is remarkably sensitive to the curve’s initialization.

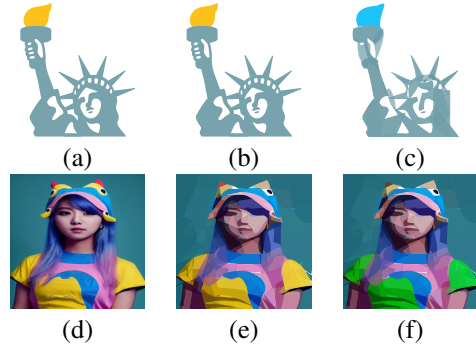


Figure 18: **Color Editing.** We use O&R to vectorize the raster images: (a) / (d) to (b) / (e) respectively. Subsequently, we perform color edits on the Bézier shapes to obtain the color-edited images shown in (c) / (f).

T-Shirt. In this case, multiple shapes were involved, but only the colors were changed. The underlying shape structure remained unaltered. As shown, our topology-aware method enables straightforward image editing.

Implementation Details

We give a detailed description of the implementation details.

DBSCAN: We use DBSCAN to cluster image colors. The DBSCAN parameters are fixed to $\epsilon = 5$ gray levels, and $\text{min_points} = 20$. Since there is much redundancy in color space, it is enough to resize the image to 100×100 pixels and run DBSCAN on the decimated image. The cluster centers association is then projected back at the 240×240 image. An $\epsilon = 5$ defines the distance in gray levels between points such that they are in the same neighborhood. $\text{min_points} = 20$ has implication on the smallest area for a connected component which is $20 \cdot \frac{240}{100} = 48$ pixels.

Optimization: We use the publicly available DiffVG implementation and its Pythonic interface. For qualitative evaluation, we follow (Ma et al. 2022) and reshape images to 240×240 . To optimize shape parameters, we use two instances of Adam (Kingma and Ba 2014) optimizers: one

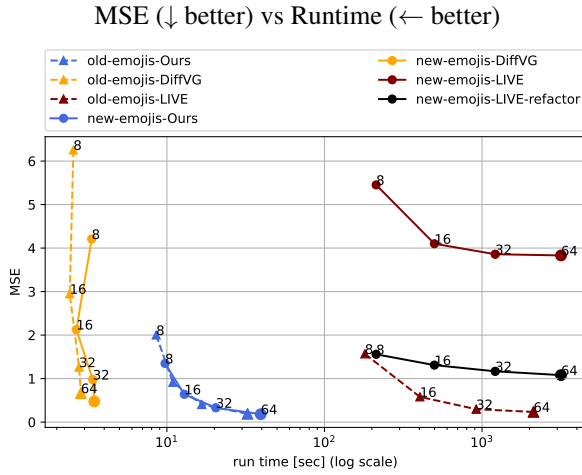


Figure 19: **MSE vs Runtime for the two Emojis datasets:** Colors code the different methods: DiffVG in yellow, LIVE in maroon and Ours in royal-blue. Triangles code the old emojis dataset and dots represent the new emojis dataset. The black line shows LIVE’s result after we fixed their preprocessing bug. After the fix, we can see that our method reflects competitive results compared to LIVE for a low shapes budget. We can observe a MSE gap of 3 gray levels.

with a learning rate of 1.0 for the Bézier coordinates and the other, with a learning rate 10^{-2} to optimize for the RGBA parameters. Throughout the paper, we use $\mathcal{L}_{optimize} = \text{MSE}$ for quantitative evaluation. For qualitative evaluation we use the combination of L_1 and CLIP loss and our geometric loss: $\mathcal{L}_{optimize} = \alpha L_1 + (1 - \alpha) \mathcal{L}_{CLIP}$

Reduce: Our Reduce steps follow an exponential decay schedule, that is, the number of shapes is halved in each iteration. We evaluate four optimization steps and three reduction steps. Midjourney target shapes are 32, 64, 128, 512 and for the rest of the datasets, we follow LIVE (Ma et al. 2022) for target shapes of 8, 16, 32 and 64.

Geometric Loss: Our geometric loss has two hyperparameters: $\lambda_{geometric}$ which weighs the contribution of the geometric loss for the optimization loss. Another is λ_p which controls the balance between our intersubsections regularizer and the orientation regularizer. In cases where the geometric loss is incorporated, we set its hyperparameters to $\lambda_{geometric} = 0.01$ and $\lambda_p = 10$.

Code: The evaluation of the optimization-based methods was conducted using their publicly available implementation.³⁴ We found a bug in LIVE’s image loading process which degrades its performance when switching from the old emojis dataset to the new emojis dataset. When this bug was fixed, the MSE for 8 shapes was reduced from 5.3 gray levels to 1.5 gray levels. The bug-fix and Our methods im-

plementation will be published. Figure 19 shows the MSE gap between the case with and without our bug-fix. We run our competitors using default parameters stated by the authors.

Benchmark Evaluation: Our goal for benchmark evaluation is to evaluate both the quality of reconstruction and the runtime of three methods: DiffVG, LIVE and Ours. For reconstruction error we use both pixel-wise (MSE) and Perceptual (LPIPS) losses for evaluation. As for runtime considerations, we run all three methods on an NVIDIA RTX A5000 GPU, i7-13700K CPU with Ubuntu 22.04.2 LTS. We evaluate the runtime performance of DiffVG, LIVE, and our method. As DiffVG converges quickly to a pleasing solution, a fixed number of optimization iterations is unfair for runtime comparison. Thus, we introduce the following three conditions for the number of iterations: (1) an upper bound of 500 iterations, (2) a lower bound of 50 iterations, and (3) an early-stopping criteria, where we stop the optimization if the loss does not improve by 0.01% from the previous iteration. For our method, we allocate a total of 500 iterations, spread across four steps: 150, 100, 100, and 150 iterations, respectively. We fix some bugs in the official LIVE implementation and modify it to support early stopping, for fair comparisons.

Early Stopping: We observed that DiffVG exhibits inconsistent convergence times across different images. The convergence time tends to increase with image complexity and the number of shapes involved. To address this issue, we propose an early stopping mechanism for DiffVG’s optimization process. Specifically, we suggest a lower bound of 50 iterations and an upper bound of 500 iterations. Additionally, we monitor the loss function during optimization and halt the process if the loss fails to decrease by more than $10^{-2}\%$ compared to the previous iteration’s loss value. To determine this threshold, we empirically analyzed the rate of loss decrease for multiple images and selected the value at which a non-monotonic decrease in loss improvement becomes apparent. We have implemented early stopping for both DiffVG and Our method, as mentioned earlier. In the case of LIVE, we provide two evaluations: (1) LIVE with 500 iterations per shape, and (2) LIVE with early stopping (LIVE-ES), utilizing a total of 500 iterations. We have observed that LIVE terminates the optimization procedure once it reaches the minimum threshold of iteration steps. This behavior can be attributed to the slow convergence of LIVE’s UDF loss towards the final shape. The gradual convergence leads to relatively small improvements in the loss from one iteration to the next, causing it to fall below the improvement condition for our early-stopping mechanism.

Geometric Loss

We refer the reader to Figure 20. Using the same mathematical formulation of cubic Bézier curve (in order: A, B, C, and D) and using the orientation function ($O(A, B, C)$) as defined in the main paper, we can verify the same orientation for [A, B, C] and [B, C, D], or check whether AB intersects CD. First, we define the soft Boolean functions AND and

³<https://github.com/BachiLi/diffvg>

⁴<https://github.com/Picsart-AI-Research/LIVE-Layerwise-Image-Vectorization>

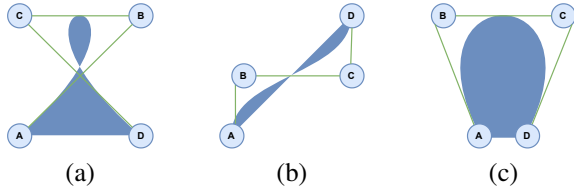


Figure 20: **Geometric Loss:** Our geometric constraint prevents curve intersubsections, resulting in the smoother topology of shapes. Our geometric loss term has three components, each one aiming to eliminate intersubsection cases: (b) Self-intersubsection occurs when AB intersects CD . In addition, Cross-intersubsections are prone to happen when: (c) $[A, B, C]$ and $[B, C, D]$ have different orientations. (d) $\angle ABC$ or $\angle BCD$ are acute.

XOR:

$$AND(A, B) = A \cdot B \quad (10)$$

$$XOR(A, B) = A + B - (A \cdot B) \quad (11)$$

Using these functions, the same orientation for $[A, B, C, D]$ can be defined as:

$$f_{orientation}(A, B, C, D) = AND(O(A, B, C), O(B, C, D)) \quad (12)$$

And the intersubsection of AB and CD occurs when:

$$f_{intersect}(A, B, C, D) = AND(XOR(O(A, B, C), O(A, B, D)), XOR(O(C, D, A), O(C, D, B))) \quad (13)$$

In cases where the geometric loss is incorporated, we set its hyperparameters to $\lambda_{geometric} = 0.01$ and $\lambda_p = 10$.

Quantitative Results: LPIPS

We evaluate the performance of our approach using two quantitative reconstruction metrics: (1) Mean Squared Error (MSE), as presented in the main paper, and (2) LPIPS (Learned Perceptual Image Patch Similarity) (Zhang et al. 2018), a perceptual similarity metric that measures the similarity between two images. LPIPS leverages feature embeddings extracted from a VGG network [2] to compute the similarity between images. In Figure 21, we depict the LPIPS score reconstruction error plotted against the number of shapes in the vector representation, with each method distinguished by a different color. Across all datasets, our method consistently surpasses DiffVG in terms of reconstruction quality when considering an equal number of shapes.

Further Results

Vectorization: Figure 24 presents a qualitative comparison of DiffVG, LIVE, and our method for the vectorization task on the old emojis dataset. Figure 25 showcases comparisons between DiffVG and Our method for vectorization on the NFT-Apes dataset. Additionally, Figure 26 displays vectorization results of images from the Midjourney dataset.

Image Abstraction: In accordance with the approach presented in (Vinker et al. 2022a), we showcase various levels of abstraction in our images. We achieve image abstraction by (1) varying the number of shapes in the vector representation and (2) adjusting a hyperparameter α , which governs the balance between the L_1 loss and CLIP loss. We suggest using three CLIP loss terms: The first term describes the global image-to-image embedding loss - which reflects a contextualized term. The second term encourages low-level features extracted from the CLIP encoder to match. The third term encourages the prompt (text) embedding and the image embedding to match. E is the image encoder, E_t is the text encoder and $E^{(\ell)}$ is the attention map of the ℓ -th layer.

$$\begin{aligned} \mathcal{L}_{clip} = & \text{dist}\left(E(I), E(\hat{I})\right) \\ & + \lambda_{CLIP-geo} \cdot \sum_{\ell} \left| E^{(\ell)}(I) - E^{(\ell)}(\hat{I}) \right|_2 \quad (14) \\ & + \lambda_{CLIP-text} \cdot \text{dist}\left(E_t(\text{text}), E(\hat{I})\right) \end{aligned}$$

We illustrate the individual effects of varying α and the number of shapes in Figure 23. Additionally, we showcase the combined effect of adjusting both parameters in Figure 22. We kindly ask the reader to zoom in for details.

Interpolation: We provide more examples of emojis interpolation in Figure 27. We ask the reader to zoom in for details.

Datasets Showcase and Specifications

Table 1 explicitly report the images names from the two versions of Noto-Emojis dataset that we collect. The new emojis dataset supports different resolutions: 32×32 , 72×72 , 128×128 , 512×512 . We randomly selected images from all resolutions. The top subsection of Table 1 shows the emojis names and their resolutions in a *resolution/emojis.filename* format. The bottom subsection of Table 1 lists the emojis names collected from the old version of Noto-Emojis.

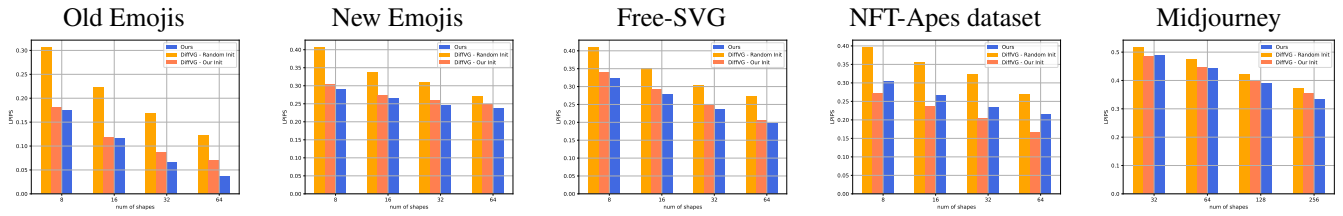


Figure 21: **LPIPS vs Number of shapes:** Top row: MSE reconstruction error (\downarrow better) vs the number of shapes in the vector representation. Bottom row: LPIPS score (\downarrow better) vs the number of shapes. Our method consistently outperforms DiffVG for all datasets. Note that for the NFT-Apes dataset, our initialization imposes an inductive bias that slightly improves the performance of DiffVG when used in conjunction with our initialization.

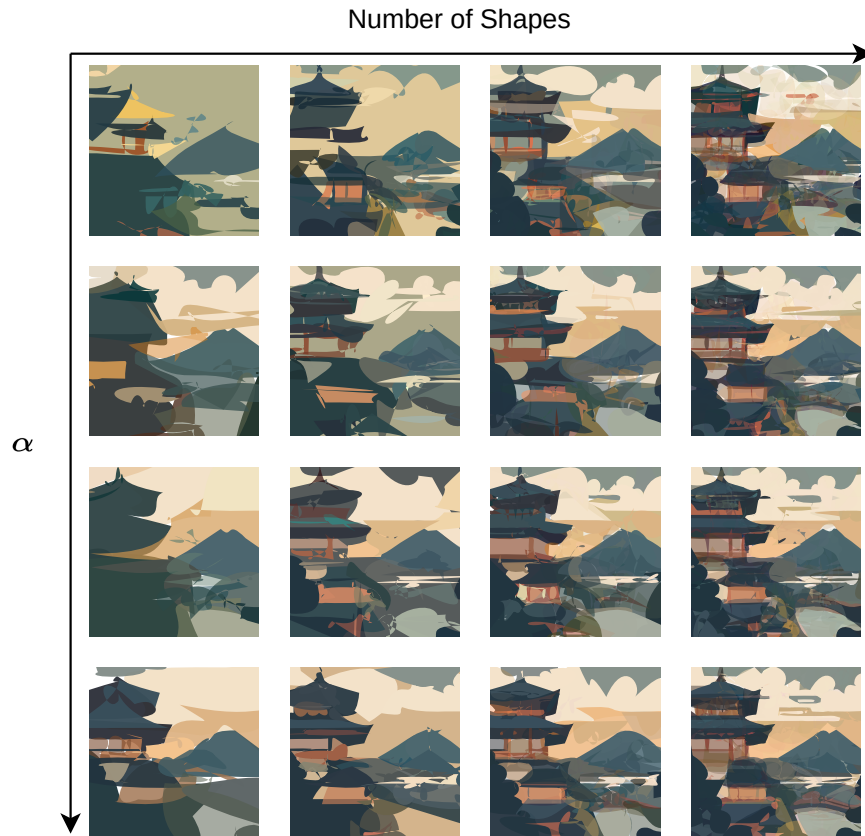


Figure 22: **Abstraction Matrix:** Results obtained for a single input image using various values of α and number of shapes. α is the hyperparameter for $\mathcal{L}_{optimize} = \alpha L_1 + (1 - \alpha) \mathcal{L}_{CLIP}$.

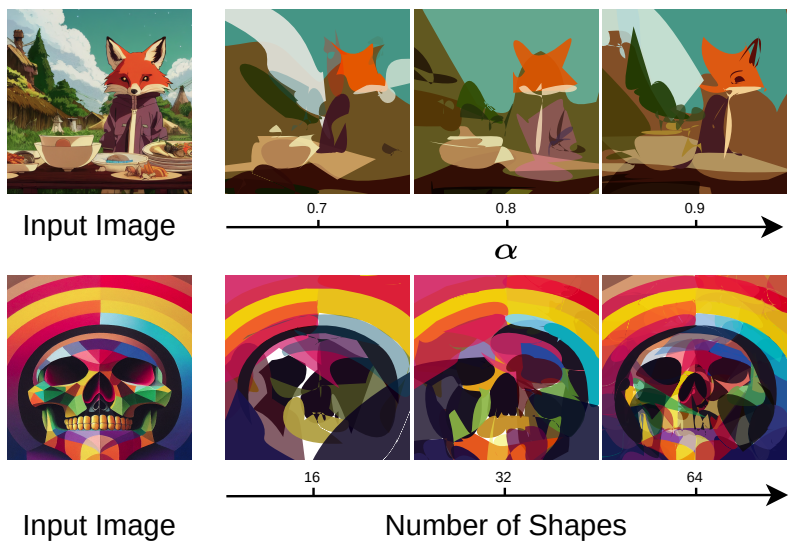


Figure 23: **Abstraction Examples:** Examples of different levels of abstraction using various α values and number of shapes. Lower α means more abstraction

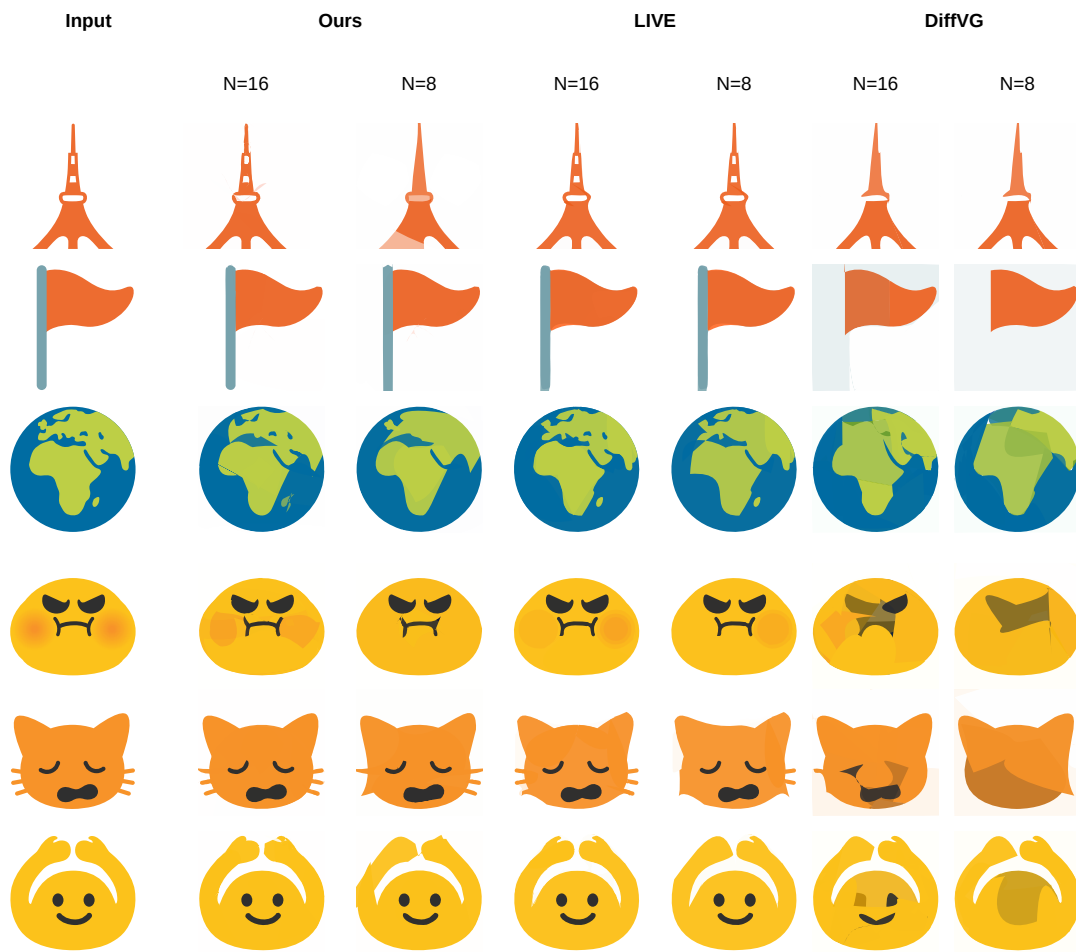


Figure 24: **Qualitative Comparison:** We showcase the results of DiffVG, LIVE, and Our method on a collection of images from the former version of EMOJI dataset. Each image is compared using the same number of shapes.

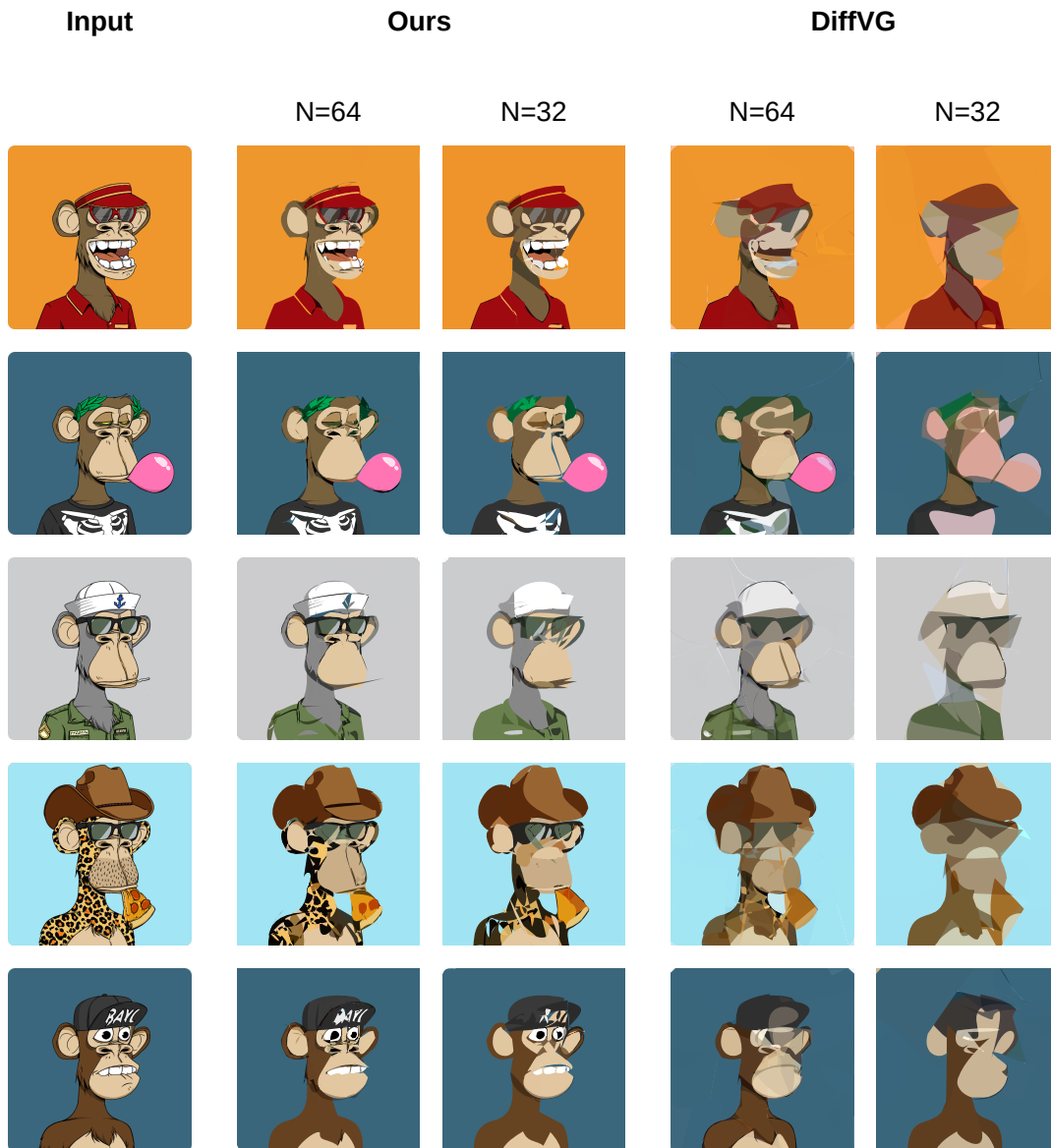


Figure 25: **Qualitative Comparison:** We showcase the results of DiffVG and Our method on a collection of images from NFT-Apes dataset.

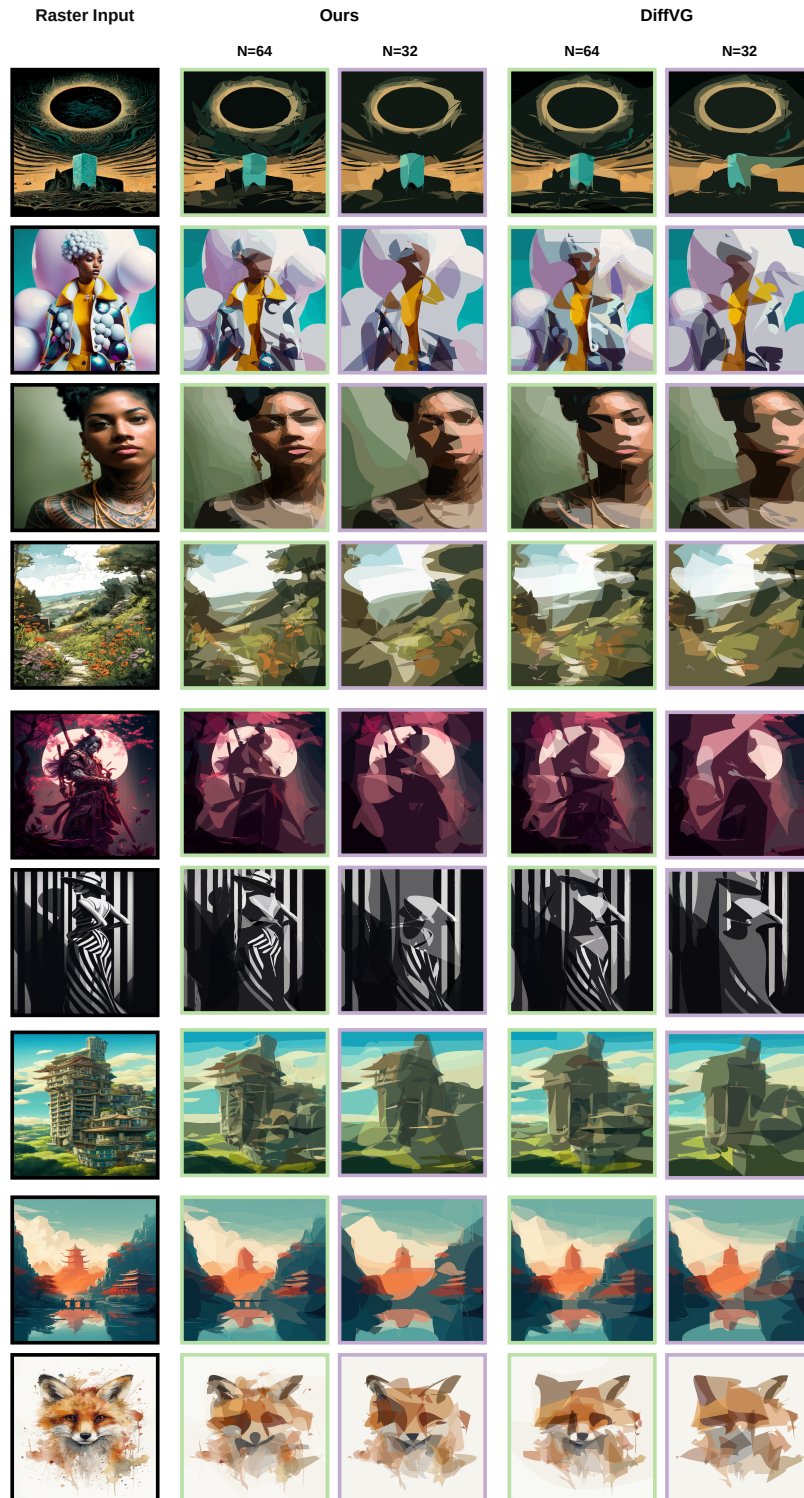


Figure 26: **More Results:** We showcase more results of our method on a collection of images generated using Midjourney. Each image is vectorized using 64/32 shapes. (colored green and violet respectively)

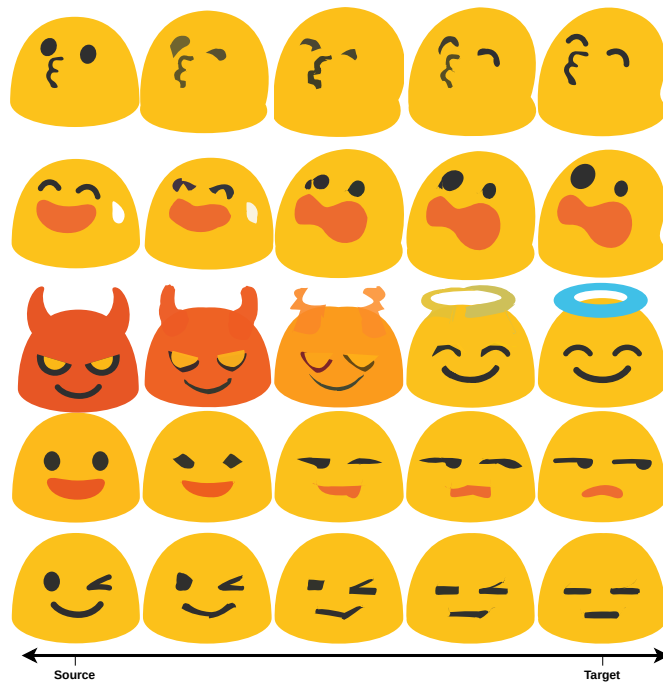


Figure 27: **Interpolation:** We perform an interpolation of emoji images from the rightmost column to the leftmost column. The initialization of the rightmost emoji is based on the vectorized result of the leftmost emoji. The intermediate images shown in between represent the optimization process's incremental results. These constitute interpolated states between the source and the target images..

32/emoji.u1f609	512/emoji.u1f60c	32/emoji.u1f637	72/emoji.u1f619	512/emoji.u1f620
512/emoji.u1f630	128/emoji.u1f620	128/emoji.u1f913	32/emoji.u1f62f	72/emoji.u1f62b
32/emoji.u1f629	32/emoji.u1f627	32/emoji.u1f62a	32/emoji.u1f603	72/emoji.u1f603
72/emoji.u1f62a	72/emoji.u1f612	512/emoji.u1f605	32/emoji.u1f605	72/emoji.u1f970
72/emoji.u1f623	512/emoji.u1f61f	512/emoji.u1f606	128/emoji.u1f62e	128/emoji.u1f627
128/emoji.u1f912	32/emoji.u1f635	32/emoji.u1f643	512/emoji.u1f631	72/emoji.u1f632
128/emoji.u1f61c	128/emoji.u1f612	128/emoji.u1f60a	512/emoji.u1f912	72/emoji.u1f610
128/emoji.u1f613	32/emoji.u1f60f	32/emoji.u1f61f	32/emoji.u1f917	72/emoji.u1f625
72/emoji.u1f616	72/emoji.u1f975	128/emoji.u1f925	128/emoji.u1f917	512/emoji.u1f611
32/emoji.u263a	128/emoji.u1f632	512/emoji.u1f641	128/emoji.u1f62b	128/emoji.u1f644
512/emoji.u1f61d	512/emoji.u1f642	512/emoji.u1f602	32/emoji.u1f621	512/emoji.u1f615
128/emoji.u1f630	128/emoji.u1f607	32/emoji.u1f620	32/emoji.u1f607	32/emoji.u1f613
72/emoji.u1f60b	128/emoji.u1f636_200d_1f32b	32/emoji.u1f611	128/emoji.u1f61f	32/emoji.u1f911
32/emoji.u1f618	32/emoji.u1f62e	32/emoji.u1f600	128/emoji.u1f606	32/emoji.u1f622
128/emoji.u1f634	72/emoji.u1f62f	72/emoji.u1f617	512/emoji.u1fae2	128/emoji.u1f61a
72/emoji.u1f62c	72/emoji.u1f609	72/emoji.u1f605	72/emoji.u1f971	512/emoji.u1f637
512/emoji.u1f913	128/emoji.u1f619	32/emoji.u1f633	32/emoji.u1fae8	512/emoji.u1f914
128/emoji.u1f636	72/emoji.u1f60f	72/emoji.u1f600	72/emoji.u1f635_200d_1f4ab	32/emoji.u1f913
72/emoji.u1f642	512/emoji.u1f973	128/emoji.u1f605	72/emoji.u1f613	512/emoji.u1f970
128/emoji.u1f629	72/emoji.u1f620	72/emoji.u1f611	512/emoji.u1f627	32/emoji.u1f636_200d_1f32b
32/emoji.u1f631	32/emoji.u1fae0	512/emoji.u1f618	512/emoji.u1f62d	512/emoji.u1f634
512/emoji.u1f636	512/emoji.u1f62f	32/emoji.u1f610	72/emoji.u1fae0	512/emoji.u1f62b
512/emoji.u1f910	72/emoji.u1f60c	512/emoji.u1f600	32/emoji.u1f62c	512/emoji.u1f60d
512/emoji.u1f628	32/emoji.u1f614	128/emoji.u1f910	32/emoji.u1f628	32/emoji.u1f616
32/emoji.u1f60b	128/emoji.u1f626	72/emoji.u1f915	512/emoji.u1f915	512/emoji.u1f925
128/emoji.u1f642	72/emoji.u1f634	72/emoji.u1f644	72/emoji.u1f636	128/emoji.u1f974
72/emoji.u1f622	128/emoji.u1f621	128/emoji.u1f975	32/emoji.u1f972	72/emoji.u1f637
32/emoji.u1f61a	512/emoji.u1fae0	72/emoji.u1f629	32/emoji.u1f974	512/emoji.u1f632
512/emoji.u1f644	128/emoji.u1f631	512/emoji.u1f61c	512/emoji.u1f60e	512/emoji.u1f60f
72/emoji.u1f633	512/emoji.u1f923	128/emoji.u1f633	128/emoji.u1f617	72/emoji.u1f604
emoji.u1f6af	emoji.u1f3a7	emoji.u1f5ff	emoji.u1f631	emoji.u1f6a4
emoji.u1f6ae	emoji.u1f627	emoji.u1f6a2	emoji.u1f478	emoji.u1f474
emoji.u1f618	emoji.u1f637	emoji.u1f6b0	emoji.u1f1ec_1f1e7	emoji.u1f30e
emoji.u1f4fc	emoji.u1f622	emoji.u1f31e	emoji.u1f3a8	emoji.u1f6a8
emoji.u1f602	emoji.u1f1ea_1f1f8	emoji.u1f473	emoji.u1f612	emoji.u1f6a3
emoji.u1f605	emoji.u1f6a0	emoji.u1f6b2	emoji.u1f4fb	emoji.u1f6a6
emoji.u1f639	emoji.u1f6b1	emoji.u1f635	emoji.u1f472	emoji.u1f3a4
emoji.u1f640	emoji.u1f33c	emoji.u1f603	emoji.u1f479	emoji.u1f611
emoji.u1f33a	emoji.u1f6ab	emoji.u1f31b	emoji.u1f620	emoji.u1f604
emoji.u1f1ee_1f1f9	emoji.u1f609	emoji.u1f31f	emoji.u1f636	emoji.u1f632
emoji.u1f614	emoji.u1f621	emoji.u1f5fe	emoji.u1f638	emoji.u1f476
emoji.u1f467	emoji.u1f30f	emoji.u1f628	emoji.u1f33d	emoji.u1f31a
emoji.u1f634	emoji.u1f6aa	emoji.u1f633	emoji.u1f648	emoji.u1f3a1
emoji.u1f6a9	emoji.u1f33e	emoji.u1f624	emoji.u1f645	emoji.u1f626
emoji.u1f475	emoji.u1f3a3	emoji.u1f470	emoji.u1f623	emoji.u1f6ac
emoji.u1f30c	emoji.u1f601	emoji.u1f468	emoji.u1f617	emoji.u1f3a5
emoji.u1f1ef_1f1f5	emoji.u1f33f	emoji.u1f469	emoji.u1f608	emoji.u1f471
emoji.u1f616	emoji.u1f649	emoji.u1f3a2	emoji.u1f5fd	emoji.u1f629
emoji.u1f646	emoji.u1f477	emoji.u1f6a7	emoji.u1f1eb_1f1f7	emoji.u1f666
emoji.u1f31d	emoji.u1f34b	emoji.u1f30d	emoji.u1f610	emoji.u1f34a
emoji.u1f31c	emoji.u1f5fb	emoji.u1f6a1	emoji.u1f606	emoji.u1f6ad
emoji.u1f647	emoji.u1f30b	emoji.u1f5fc	emoji.u1f6b3	emoji.u1f625
emoji.u1f615	emoji.u1f600	emoji.u1f6a5	emoji.u1f3a0	emoji.u1f33b
emoji.u1f619	emoji.u1f613	emoji.u1f3a6	emoji.u1f630	emoji.u1f607

Table 1: **Emoji Dataset:** File names from noto-emoji dataset used for evaluation: (Top) new format, (Bottom) old format. The format of the new emojis dataset is resolution/emoji_filename.

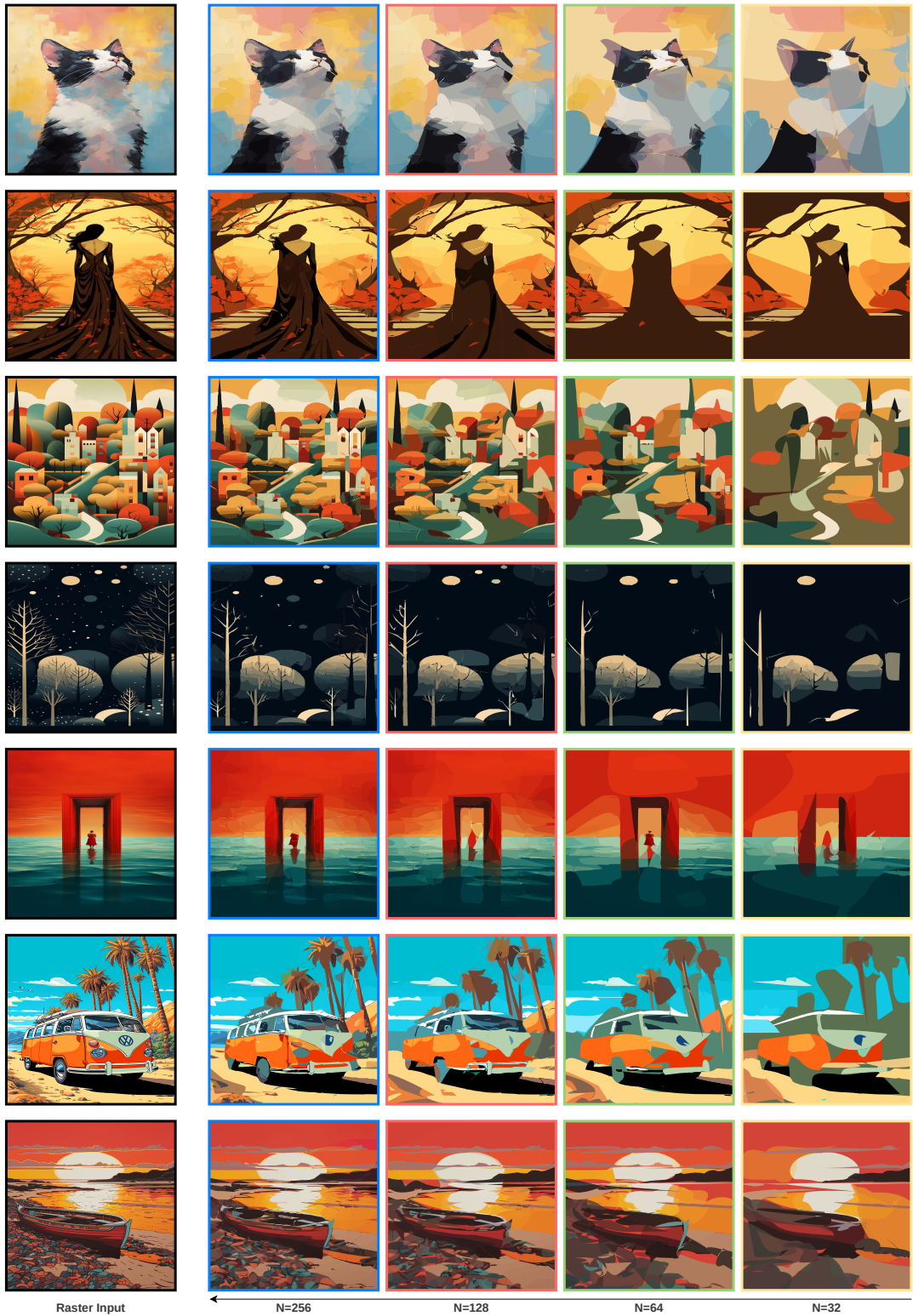


Figure 28: **Additional Results:** We showcase more results of our method on a collection of images generated using Midjourney. Each image is vectorized using 256, 128, 64, and 32 shapes (shown in blue, red, green, and yellow, respectively).